Biosensors and Bioelectronics 53 (2014) 486–493

Contents lists available at ScienceDirect

Biosensors and Bioelectronics

journal homepage: www.elsevier.com/locate/bios

A size selective porous silicon grating-coupled Bloch surface and sub-surface wave biosensor

Gilberto A. Rodriguez *[,1], Judson D. Ryckman [1], Yang Jiao, Sharon M. Weiss

Department of Electrical Engineering and Computer Science, Vanderbilt University, VU Station B #351824, 2301 Vanderbilt Place, Nashville, TN 37235-1824, United States

ARTICLE INFO

Article history:
Received 5 August 2013
Received in revised form
11 October 2013
Accepted 15 October 2013
Available online 23 October 2013

Keywords:
Porous silicon
Bloch surface wave
Bloch sub-surface wave
Biosensor
Size-selective

ABSTRACT

A porous silicon (PSi) grating-coupled Bloch surface and sub-surface wave (BSW/BSSW) biosensor is demonstrated to size selectively detect the presence of both large and small molecules. The BSW is used to sense large immobilized analytes at the surface of the structure while the BSSW that is confined inside but near the top of the structure is used to sensitively detect small molecules. Functionality of the BSW and BSSW modes is theoretically described by dispersion relations, field confinements, and simulated refractive index shifts within the structure. The theoretical results are experimentally verified by detecting two different small chemical molecules and one large 40 base DNA oligonucleotide. The PSi-BSW/BSSW structure is benchmarked against current porous silicon technology and is shown to have a 6-fold higher sensitivity in detecting large molecules and a 33% improvement in detecting small molecules. This is the first report of a grating-coupled BSW biosensor and the first report of a BSSW propagating mode.

1. Introduction

Optical biosensors offering label-free detection of relevant chemical species with high sensitivity, rapid read-out, and low-cost are essential for applications spanning medical diagnostics, food safety, and homeland security. For detection of specific label-free bioanalytes and small molecules, plasmonic and photonic sensing platforms have emerged as powerful tools (Adhikari and Majumdar, 2004; Homola et al., 2005; Jane et al., 2009; Kang et al., 2012; Maxwell et al., 2002). In these platforms, the immobilization of an analyte creates a measureable change in the optical properties of the structure, often due to a change in refractive index at the surface of the sensor that is probed by an evanescently decaying field. Because conventional optical platforms utilize planar solids, the total number of available surface binding sites for analytes is limited and there is only minor interaction of the optical field and analyte at the bulk surface, resulting in limited sensitivity. Furthermore, sensors based on planar solid materials are unable to size selectively filter unwanted material or size selectively detect target molecules.

Porous sensing structures address many of the aforementioned challenges and are increasingly being incorporated into optical sensing platforms (Feng et al., 2011; Jane et al., 2009; Jones and Porter, 1988). Porous silicon (PSi) is a particularly attractive label-free biosensing platform due to its highly tunable optical properties, enhanced surface area, and rapid and cost-effective fabrication. The large surface area, arising from the presence of nanoscale pores, allows for improved sensitivity to biomolecule interactions, while the tunable pore dimensions ($\sim$2 nm to $>$100 nm) enable size-selective detection and filtration of larger contaminant species (Lawrie et al., 2010). Label free sensing can be performed through optical transduction schemes and has been demonstrated in a wide variety of PSi optical structures such as single-layer and double-layer interferometers (Dancil et al., 1999; Pacholski et al., 2005), Bragg mirrors (Snow et al., 1999), rugate filters (Li et al., 2012), microcavities (Chan et al., 2000), waveguides (WG) (Rong et al., 2008; Wei et al., 2012; Wei and Weiss, 2011), Bloch surface wave (BSW) structures (Guillermain et al., 2007; Jamois et al., 2010; Michelotti et al., 2010; Qiao et al., 2010), and diffraction gratings (Ryckman et al., 2010). These PSi optical structures have been demonstrated to perform high sensitivity and label-free detection of small proteins, DNA, and other biologically important analytes.

One key limitation facing PSi sensors is the ability to effectively detect both small molecules that can easily infiltrate the porous matrix and large molecules that either slowly diffuse into or are filtered out by the pores. Among the demonstrated porous sensor platforms, the BSW structure holds great promise for sensitively detecting large molecules on the surface of the sensor. The BSW is an optical surface state characterized by distinct field confinement at the interface between a finite 1D photonic crystal, or Bragg mirror, and an external semi-infinite medium (Guillermain et al., 2007;

* Corresponding author. Tel.: +615 345 8311; fax: +615 343 6702.
E-mail address: gilberto.a.rodriguez@vanderbilt.edu (G.A. Rodriguez).
[1] These authors contributed equally.

0956-5663/$ - see front matter © 2013 Elsevier B.V. All rights reserved.
http://dx.doi.org/10.1016/j.bios.2013.10.028

Liscidini and Sipe, 2009; Qiao et al., 2010). The BSW is often considered to be the dielectric analog to the surface plasmon polariton (SPP), which provides a strong propagating field at the dielectric-metal interface due to the surface electron oscillation (Descrovi et al., 2010; Liscidini et al., 2009). With the SPP, however, waves propagate along a lossy gold or silver surface and thus have limited propagation lengths and resonant quality factors, considerably lower than what can be achieved with all-dielectric BSW designs (Descrovi et al., 2010; Liscidini et al., 2009; Sinibaldi et al., 2012). Thus, the BSW has emerged as a promising sensing platform for surface-bound molecule detection and has been experimentally demonstrated in various material platforms (Descrovi et al., 2010; Konopsky and Alieva, 2007; Pirotta et al., 2013; Qiao et al., 2010; Toma et al., 2013). Through the use of a porous dielectric, the accessible surface area of a BSW structure can be increased significantly, which promotes improved sensitivity toward small molecules (Descrovi et al., 2010; Guillermain et al., 2007; Jamois et al., 2010; Konopsky and Alieva, 2007; Liscidini et al., 2009; Michelotti et al., 2010; Paeder et al., 2011; Qiao et al., 2010).

In this article, we present a label-free method for size-selective sensing of both small (<2 nm) and large (~ 10 nm) low molecular weight molecules (<15 kDa) using grating-coupled BSW and Bloch sub-surface wave (BSSW) optical modes of a PSi multilayer. The BSW is confined at the multilayer–air interface, which is advantageous for high sensitivity, rapid detection of larger molecules that have difficulty infiltrating the porous matrix. The BSSW, first introduced in this work, is confined just beneath the surface and has a strong sensitivity to small molecules that penetrate the porous matrix. By utilizing a one-dimensional integrated grating at the surface of the structure, coupling can be achieved by far field excitation at a unique resonant angle (Ryckman et al., 2010; Wei and Weiss, 2011) while also eliminating the need for a bulky prism and air gap tuning (Rong et al., 2008). The grating-coupled PSi-BSW/BSSW platform is benchmarked against a grating-coupled PSi-WG (Wei and Weiss, 2011) and demonstrates a larger sensitivity to both small and large molecules.

2. Materials and methods

2.1. Fabrication of BSW/BSSW and WG sensors

The porous silicon structures were fabricated by electrochemical etching of p+ ($\sim 0.01\ \Omega$ cm) Si(1 0 0) wafers. By placing the silicon in a solution containing 15% HF in ethanol and varying the applied current density and duration, the resulting PSi layer thickness and porosity can be tuned. Table 1 shows the current densities and times used to fabricate the structures used in this work. A two second etch break (no current applied) is employed between the formation of each layer. The etching parameters were chosen based on rigorous coupled wave analysis (RCWA) simulations to yield structures with clear optical resonances (Moharam et al., 1995). The etched samples were placed in a 1.5 mM L^{-1} KOH in ethanol solution for 5 min to widen the pores for enhanced molecule infiltration. The samples were then thermally oxidized in air ambient at 500 °C for 5 min. The nominal refractive index of each layer is approximated by fitting the measured reflectivity spectrum of the layer with a thin film simulation that incorporates the scanning electron microscopy (SEM) measured thickness of the layer. For the BSW/BSSW sensor, reflectance spectra of the entire structure were used to fit the multilayer refractive index gradient that gives rise to the BSSW mode. The refractive index gradient was linearly varied from $n_{i1}=1.62$–1.72 and $n_{i2}=1.22$–1.26 for the low current density and high current density layers, respectively. We found that our combination of standard etching, brief KOH treatment, and oxidation produces a natural and reproducible gradient in the optical properties of the multilayer, although the necessary refractive index profile could also be formed by appropriately tuning the PSi etching conditions. We postulate that the dominant contribution to the natural gradient refractive index arises from the diffusion time of the KOH and the duration of KOH exposure to the PSi membrane. This hypothesis is supported by additional tests performed on BSW/BSSW samples with different KOH exposure times for which the BSSW resonance was either not visible or shifted to different angles.

The grating couplers were fabricated by electron beam lithography (EBL). ZEP 520A resist was spun at 6000 rpm to create a ~ 300 nm thick layer and then patterned using a Raith eLine EBL tool. The WG and BSW couplers have grating pitches of $\Lambda_{WG}=1590$ nm and $\Lambda_{BSW/BSSW}=1820$ nm, respectively. After development, the grating duty cycles were measured to be approximately 66% (air: silicon).

Table 1
Electrochemical etching parameters used for device fabrication.

Structure	Layer	Current density (mA/cm^2)	Time (S)	Refractive index	Thickness (nm)
BSW/ BSSW	d_{01}	5	34	Gradient from 1.62 to 1.78	175
	d_{i1} for $i=1$ to 10	5	63		340
	d_{i2} for $i=0$ to 10	48	22	Gradient from 1.22 to 1.26	580
WG	d_{wg}	5	65	1.79	345
	$d_{cladding}$	48	53	1.24	1700

2.2. Chemical preparation

Each sample was soaked in a 4% 3-aminopropyltriethoxysilane (3-APTES) solution in methanol and water for 20 min, followed by a soak in methanol for 10 min to remove the excess silane. Although 3-APTES multilayers are difficult to prevent (Zhu et al., 2012), the 10 min methanol soaking procedure enables a consistent attachment of the molecule. The samples were then thermally annealed at 100 °C for 10 min to promote cross linking between the surface silicon oxide and amino group. A 2.5 $mg \cdot mL^{-1}$ Sulfosuccinimidyl-4-(*N*-maleimidomethyl)cyclohexane-1-carboxylate (Sulfo-SMCC) in 4-(2-hydroxyethyl)-1-piperazineethanesulfonic acid (HEPES) buffer solution was incubated with the samples for 2 h at room temperature, followed by 1 h soak in HEPES solution to remove excess material. Then, 100 μM DNA, (5′-TAG-CTA-TGG-TCC-TCG-TTA-GCT-ATG-GAA-TTC-CTC-GTA-GGC-C 3′), was prepared in HEPES buffer and then mixed with the reducing agent, TCEP (tris(2-carboxyethyl)phosphine) (Pierce) in a 1:1 mixture of methanol and water. The samples were soaked in the 50 μM DNA mixture for 1 h, followed by a 30 min soak in HEPES buffer to remove unattached oligos.

2.3. Measurement technique

The BSW and WG structures were measured between exposure to the solutions discussed in Section 2.2 using a Metricon Model 2010/M Prism Coupler. The prism was removed to allow for far-field coupling. A 1550 nm laser was used as the light source in the variable angle monochromatic fringe observance (VAMFO) mode. A depiction of the setup is illustrated elsewhere (Wei and Weiss 2011).

2.4. Sensitivity definition

In general, detection sensitivity is defined by the following equation:

$$Sensitivity = \frac{d\theta}{dn} = \frac{\int_V [E(x)]^2 dx}{\int_{-\infty}^{\infty} [E(x)]^2 dx} \cdot \frac{n_V}{N} \cdot \frac{1}{\cos\,\theta} \quad (1)$$

where the first term is the field intensity confinement factor (*i.e.*, ratio between the field intensity confined in the active sensing region where most of molecules are immobilized and the field intensity distributed throughout the entire structure), n_v is the refractive index of the active sensing volume, N is the effective refractive index for each mode, and θ is the resonance angle (Jiao and Weiss 2010b). It is clear that the detection sensitivity of a given sensor depends on the initial resonance angle of the sensor; as the initial resonance angle is increased, the detection sensitivity increases. For this reason, we choose to report a normalized sensitivity for the grating-coupled PSi-WG and PSi-BSW/BSSW sensors in which we multiply the measured resonance shift by cosθ in order to provide an unbiased sensitivity based only on the electric field confinement (E(x)) and refractive index change of the structure.

3. Results and discussion

3.1. Grating-coupled PSi Bloch surface and sub-surface waves (PSi-BSW/BSSW)

Fig. 1a shows the design of the PSi-BSW/BSSW structure. The key distinction between this structure and a traditional BSW structure is the introduction of an appropriately designed gradient or defect in the optical thickness of the layers of the 1-D photonic crystal, which creates a localized region of strong optical confinement just below the terminated 1D photonic crystal surface. To the best of our knowledge, this study is the first demonstration of such a sub-surface wave mode, which we call a Bloch sub-surface wave. As explained in detail below, the BSSW is distinguished from waveguide and band edge modes and promotes both improved sensitivity and faster sensing response. The combination of BSW and BSSW modes in a PSi device thus provides a unique platform wherein larger molecules, filtered out by the pores, are readily detected with the BSW and smaller molecules passing into the pores are detected with the BSSW.

Dispersion relations and field profiles were calculated by transfer matrix theory to highlight the difference between BSSW and band edge (BE) modes. Fig. 2 illustrates the dispersion relation and field profiles for two prototypical 1D PSi-BSW/BSSW structures (without grating couplers), designed for operation at 1550 nm (~0.8 eV) and excited through the Otto configuration using a high index $n=2.5$ prism with a constant 500 nm air gap. In Fig. 2(a,c) the BSW (red) is formed at the multilayer–air interface, where the 1D photonic crystal multilayer is nominally defined with layer thicknesses $d_{i1}=340$ nm, $d_{i2}=580$ nm and refractive indices $n_{i1}=1.79$, $n_{i2}=1.24$, respectively. Here, i is an integer (0-N) indicating the period iteration. The $i=0$ period features a reduced optical thickness with $d_{01}=175$ nm, $n_{01}=1.62$, which brings the BSW mode further into the band gap and away from the BE. The BSSW (blue) is introduced by reducing the optical thickness of layer, d_{11} (*i.e.*, the first high index layer below the surface), in this case by reducing the refractive index to $n_{11}=1.62$. We refer to this particular structure as the *step index* BSSW. The step index geometry breaks the translational symmetry of the 1D photonic crystal forming a sub-surface defect state (BSSW) similar to how the multilayer–air interface of the terminated 1D photonic crystal forms a surface defect state (BSW). As shown in Fig. 2(a), the BSSW mode falls inside the BE and has a higher effective index than the BSW. The BSSW is characterized by strong field localization just below the multilayer–air interface. In the step index BSSW, the peak field is centered in layer d_{11} and rapidly decays both toward the surface and into the multilayer. This field profile is clearly distinguished from BE modes (black) wherein the field is distributed broadly across many layers deep within the multilayer (Fig. 2(c)). In previous PSi-BSW studies, the sensitivity of the BE modes to small bulk refractive index changes has been shown to be less than the BSW resonance (Qiao et al., 2010).

A BSSW mode can also be introduced by gradually changing the optical thickness of the multilayer, forming what we refer to as the *gradient index* BSSW. In the gradient index structure, the index of layers d_{i1} and d_{i2} are gradually increased from 1.62 to 1.79 and 1.22 to 1.26, respectively. This effectively produces a locally varying band edge position and introduces numerous BSSW modes within the band gap (Fig. 2(b)). The first order BSSW mode (purple) is characterized by a field distribution confined to the first few periods below the multilayer–air interface, and is akin to a BE mode that is biased toward the sensor surface. In principle, the gradient index BSSW can function in the same manner as the step index BSSW by providing a method for sensing analyte species that infiltrate the porous matrix just beneath the sensor surface. Owing to the gradual confinement provided by the gradient index structure, we anticipate that BSSWs excited in this configuration could provide sharp, high quality factor resonances, thereby

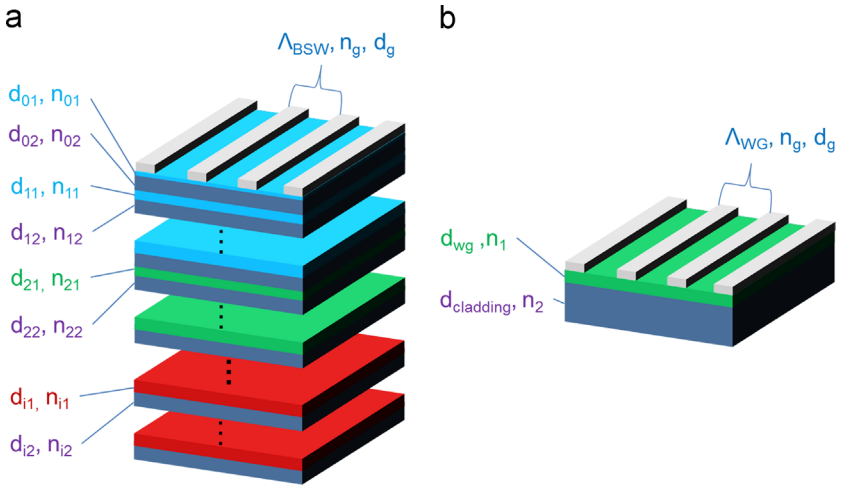

Fig. 1. Refractive index profiles of the PSi grating-coupled (a) BSW/BSSW and (b) WG sensors with corresponding thickness, d, and refractive index, n. Λ is the grating pitch.

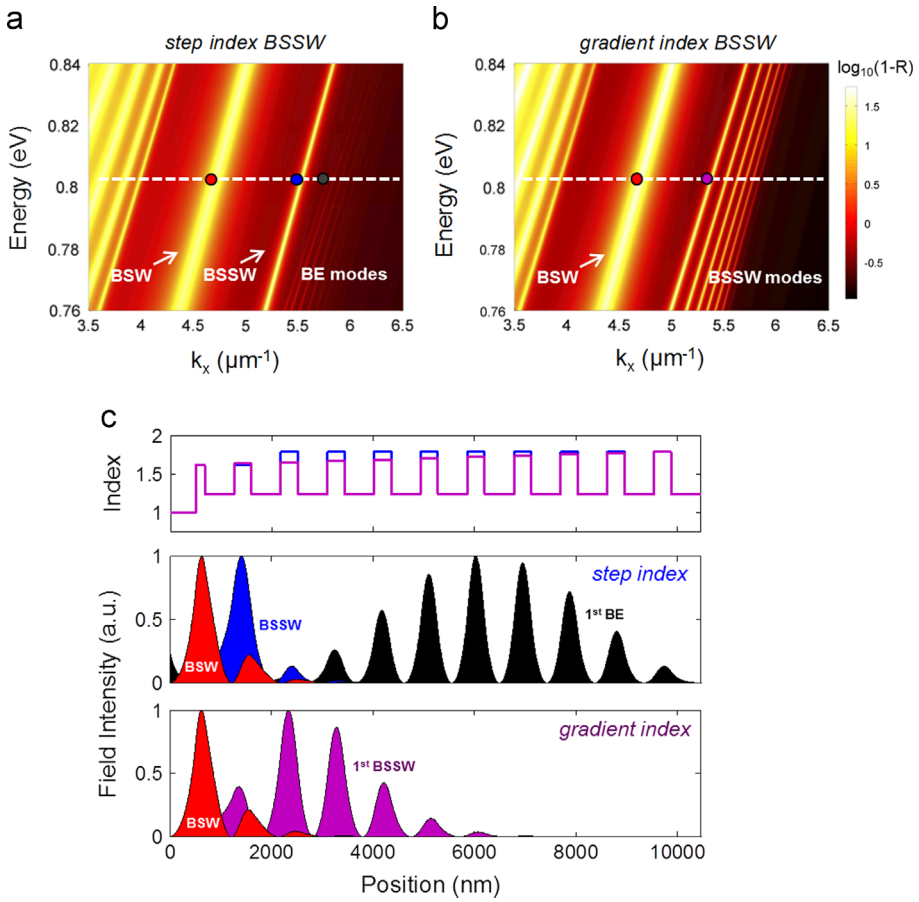

Fig. 2. Dispersion relation of the BSW/BSSW sensor for the (a) step and (b) gradient refractive index distributions. (c) Electric field confinements of the step (red/blue) and gradient (red/purple) index BSW/BSSW compared to the traditional band edge modes (black). (For interpretation of the references to color in this figure caption, the reader is referred to the web version of this paper.)

promoting improved analyte detection. This is analogous to the reduction of radiation losses caused by tapering the Bragg mirrors of a microcavity, which results in an improved quality factor (Lalanne et al., 2004). Moreover, unlike the BSW mode or modes of a PSi-WG, the BSSW is localized completely within the porous matrix, with almost no evanescent field leaking into the air cladding. This promotes increased sensitivity toward small molecules, as the BSSW can take full advantage of the increased surface area provided by the pores.

3.2. Grating-coupled PSi waveguide (PSi-WG) biosensor

Here, we briefly review the grating-coupled PSi-WG, which has recently been demonstrated as a highly sensitive, compact optical biosensor (Wei and Weiss, 2011) and will be employed in a later section for benchmarking the experimental performance of the PSi-BSW/BSSW sensor. The use of a diffraction grating coupler for the WG, similar to the BSW/BSSW structure, produces a simple, compact configuration that allows for integration of microfluidic flow cells and real-time detection of biomolecules (Wei et al., 2012). The grating-coupled PSi-WG structure consists of a high refractive index core layer, a low refractive index cladding layer, and a resist grating on top as shown in Fig. 1b. A transverse electric (TE) or transverse magnetic (TM) polarized light source directed at the grating will be diffractively coupled to the waveguide as described by Eq. (2) where n_{eff} is the effective refractive index of one WG mode, n_c is the refractive index of the cover layer, θ is the coupling angle measured from normal incidence, m is the diffraction order, λ_0 is the free space wavelength, and Λ is the grating pitch. At the coupling angle, the higher order diffracted light is strongly coupled to the high index core layer, producing a strong resonant feature in far-field reflectance (Wei and Weiss, 2011; Wei et al., 2012).

$$n_{eff} = n_c \cdot \sin\theta \pm m \cdot \frac{\lambda_0}{\Lambda} \tag{2}$$

When liquids, gases, or molecules are introduced to the structure, the refractive index of the PSi layers change, creating a detectable shift in the coupling angle, θ. Compared to non-porous sensors for which analytes only interact at the surface, the PSi-WG structure has been shown to possess a detection sensitivity one order of magnitude greater than a planar silicon-on-insulator (SOI) grating-coupled WG for the detection of 16-mer DNA (Wei and Weiss, 2011).

3.3. Modeling and theoretical performance

To demonstrate the principle functionalities of the grating-coupled PSi-BSW/BSSW sensor, rigorous coupled wave analysis (RCWA) simulations were employed (Moharam et al., 1995). The theoretical performance capabilities of the PSi-WG have been discussed elsewhere (Wei et al., 2008; Wei and Weiss, 2011). In Fig. 3, we present four example analyte sensing scenarios to demonstrate the size selective advantage for the detection of small and large molecules using the BSW/BSSW structure. The location of the BSW and BSSW peaks in air (black curve) are 21.2° and 27.5°, respectively. Here, we utilize a gradient index BSSW structure, matching the simulated fitting parameters for our experimentally fabricated grating-coupled PSi-BSW/BSSW examined later. The four scenarios (a–d) illustrated in

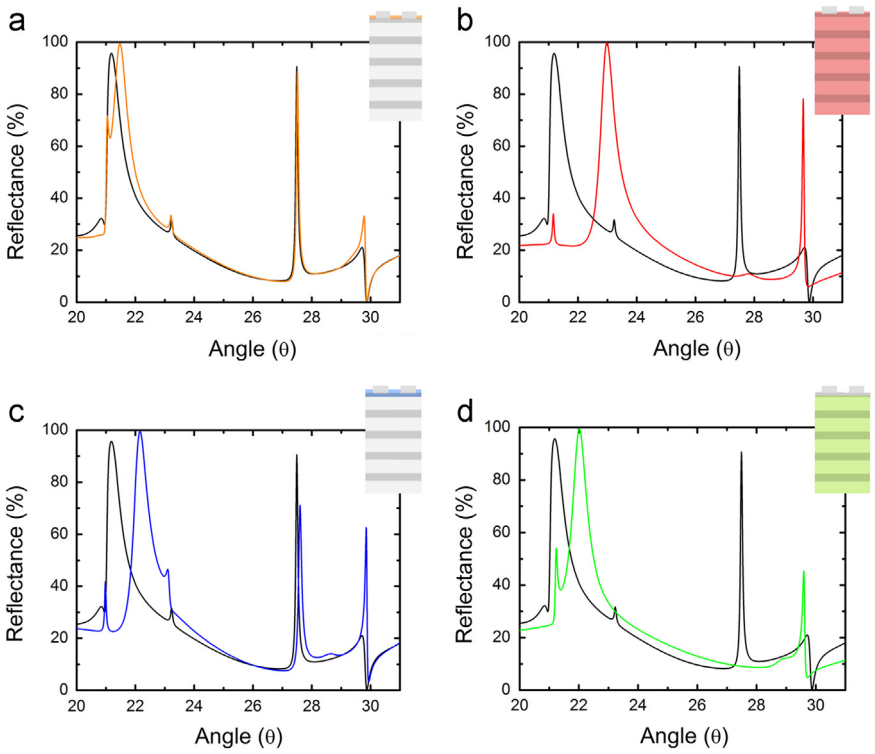

Fig. 3. Reflectance spectra shifts caused by the change in refractive index at a specified location in the BSW/BSSW sensor. (a) $\Delta n=0.5$ for 10 nm above the surface. (b) $\Delta n=0.03$ for all layers and $\Delta n=0.5$ for 10 nm above the surface. (c) $\Delta n=0.03$ for the top layer and $\Delta n=0.5$ for 10 nm above the surface. (d) $\Delta n=0.03$ for only the multilayer.

Fig. 3, represent four different analyte attachment/infiltration geometries by modeling a change in refractive index in a specific highlighted area: (a) a refractive index change, $\Delta n=0.5$, 0–10 nm above the surface of the structure, not including the grating, to simulate molecules that do not penetrate the pores, (b) a refractive index change, $\Delta n=0.03$, in the entire structure to simulate small molecules uniformly distributed within the pores in addition to large molecules, with refractive index change $\Delta n=0.5$, bound 0–10 nm above the surface, (c) a refractive index change, $\Delta n=0.03$, only in the BSW guiding layer and $\Delta n=0.5$ 0–10 nm above the surface for molecules that partially diffuse or clog the porous surface, and (d) a refractive index change, $\Delta n=0.03$, only in the multilayer to simulate a theoretical scenario where small molecules only infiltrate the multilayer region. Many chemical and biological molecules can be modeled with reasonable accuracy using a refractive index of ~1.5 (Wei and Weiss, 2011). For typical biomolecule sizes and surface densities within the porous matrix, $\Delta n=0.03$ is a typical effective index change, which may be expected following the monolayer attachment of small molecules according to the Bruggeman effective medium approximation (Khardani et al., 2007). Similarly, the displacement of air, $n=1$, by densely packed large molecules with $n=1.5$ at the surface will create an effective refractive index change of $\Delta n=0.5$ when assuming a monolayer coverage.

In Fig. 3(a), modeling large molecules attached to the surface produces a 0.31° shift in the BSW resonance and a 0.02° shift in the BSSW resonance. As expected, the magnitude of the respective resonance shifts scales with the degree of spatial overlap between each mode and the simulated molecules (see sensitivity discussion in Section 2), with the BSW mode interacting much more strongly with surface-bound molecules than the BSSW. In Fig. 3(c), a similar result is observed with slightly larger shifts for both the BSW and the BSSW due to the simulated molecule infiltration into the guiding layer as well as attachment to the surface. Note that the pore size of the guiding layer can be optimized to allow for the infiltration of large molecules without affecting the coupling of the BSW by appropriately adjusting the thickness of the layer, as previously shown (Jamois et al., 2010). Fig. 3(b) illustrates the presence of both large molecules 0–10 nm above the surface and small molecules infiltrating throughout the multilayer. The presence of both molecules induces a large resonance shift for both the BSW and BSSW. As shown in Fig. 3(d), when only the refractive index of the multilayer is changed instead of the entire structure as in Fig. 3(b), the BSW resonance shift is reduced because a smaller fraction of the BSW mode is interacting with the simulated molecules. Note that the majority of the BSW mode that extends into the porous silicon structure exists in the guiding layer and only a small fraction extends further into the multilayer; hence, the BSW resonance shifts observed in Fig. 3(c) and Fig. 3(d) are similar. Meanwhile, the BSSW resonance shift shown in Fig. 3(d) is relatively unchanged compared to the case shown in Fig. 3 (b) because the BSSW mode has no significant field extending within the top guiding layer or surface as confirmed by the lack of a significant BSSW resonance shift in Fig. 2(c). Therefore, the BSSW is not sensitive to large molecules sitting on the surface of the sensor, but the BSW can be affected by both large and small molecules within the PSi layers due to the field overlap within the first two layers of the Bragg mirror. The BSSW sensitivity derived from Fig. 3(b) is approximately 72°/RIU or 2038 nm/RIU and the large molecule sensitivities derived from the BSW shown in Fig. 3 (a,c) is approximately 0.6°/RIU (17 nm/RIU) and 31°/RIU (967 nm/RIU) for surface and top layer detection, respectively. In the next section, we demonstrate the application of our PSi-BSW/BSSW sensor.

3.4. Experimental detection of small and large molecules

Fig. 4 shows SEM images of the fabricated PSi-BSW/BSSW and PSi-WG structures used in this work. Grating couplers, constructed from ZEP 520A resist, were patterned on the surface with grating periods of 1820 nm and 1590 nm for the BSW/BSSW and WG structures, respectively. SEM imaging reveals the gratings to have

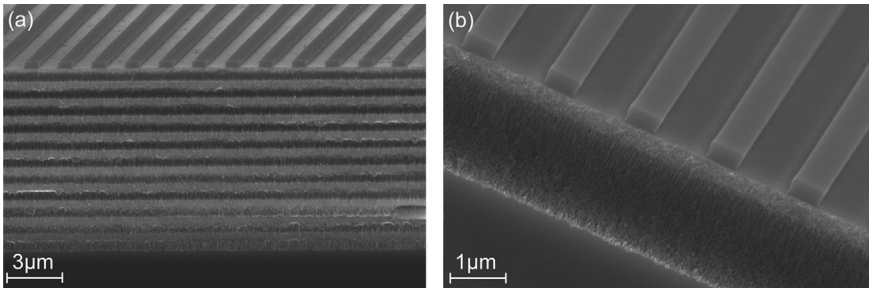

Fig. 4. SEM cross-sectional images of the (a) BSW/BSSW and (b) WG sensors.

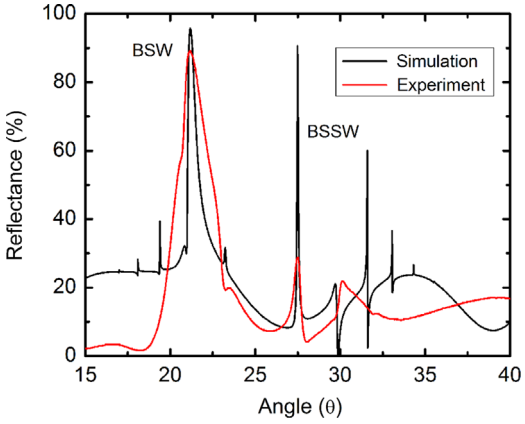

Fig. 5. Comparison of simulated and experimental performance of the BSW/BSSW sensor.

duty cycles of 66%. As discussed in Section 2, our fabrication protocol produces a gradient index type PSi-BSW/BSSW structure. The gradient refractive index is confirmed by fitting the experimental angle-interrogated reflectance with RCWA simulation. As shown in Fig. 5, the experimentally measured BSW and BSSW resonances are located at 21.2° and 27.5°, respectively. Additional BSSW modes can be seen at higher angles in both simulation and experiment. Importantly, the BSSW modes would not appear in this 28–35° angular range without the presence of a gradient or step index within the multilayer. Traditional BE modes were found in simulated structures at higher angles as demonstrated in Fig. 2.

The sensing performance of the grating-coupled BSW/BSSW and WG platforms in response to large (~10 nm) and small molecules (<2 nm) is shown in the attenuated total reflectance curves of Fig. 6(a–c). As model small molecules, 3-APTES (0.8 nm) and Sulfo-SMCC (1.26 nm) were attached in succession to the two sensor platforms (Clare and Abbott, 2005; Ouyang et al., 2006). Conveniently, these small molecules also serve as linker molecules for the immobilization of our chosen large molecule, a 13.2 nm long 40mer thiol modified probe DNA. This 40mer DNA has previously been used in studies on PSi-WGs and was shown to be unable to effectively infiltrate the ~20 nm pores of the high index PSi layers (Lawrie et al., 2010).

In this experiment, the 3-APTES and Sulfo-SMCC small molecules produce large resonance shifts (>1 degree) for all three resonant modes, indicating that they can readily penetrate the porous matrix. Note that the experimentally measured resonance shifts for the small molecule attachment in the multilayer of the BSW/BSSW sensor correspond to a gradient effective refractive index change of approximately $\Delta n = 0.03–0.05$ for 3-APTES and $\Delta n = 0.01–0.03$ for Sulfo-SMCC. Sensor sensitivity to these small molecules can be ranked by increasing order: BSW, WG, and BSSW. The BSSW shows the largest response to small molecule attachment with a 33% enhancement over the benchmark WG sensor (Fig. 6(d)).

In response to 40mer DNA attachment, the BSSW and WG show very small normalized resonance shifts of ~0.03° and ~0.05°, respectively, indicating that the large molecules are only weakly detected by these optical modes. Note that normalized resonance shifts are discussed in detail in Section 2. The BSW mode, meanwhile, shifts ~0.29°, demonstrating a ~6 fold enhancement when compared to the WG. The experimentally measured resonance shifts for DNA attachment suggest an effective refractive index change of approximately $\Delta n = 0.3$ in the region 10 nm above the surface of the BSW/BSSW sensor. If the porosity of the top layer is increased, improved molecule infiltration into the top layer may occur, leading to even higher large molecule detection sensitivity. The normalized resonant responses to large and small molecule attachment across the different sensors are summarized in Fig. 6 (d), and show that the BSW and BSSW modes exhibit the largest sensitivity to large or small molecules, respectively. As the BSW and BSSW are excited in the same structure, this importantly demonstrates size selective sensing. Specific and selective detection of target molecules using the BSW/BSSW sensor can be conducted in a similar manner as has been reported for other PSi biosensor structures. Potential applications for high accuracy specific binding events previously demonstrated in PSi biosensors include small or large DNA (Wei and Weiss, 2011), proteins (Pacholski et al., 2005), and enzymes (Qiao et al., 2010). Moreover, the enhanced sensitivity gives PSi-BSW/BSSW sensors a powerful advantage when benchmarked against the PSi-WG, which itself has previously been shown to have a significant sensitivity advantage in comparison to other platforms such as planar SOI waveguide sensors (Wei and Weiss, 2011).

4. Conclusions

In this work, we have demonstrated through simulation and experiment a grating-coupled PSi BSW sensor that supports BSSW modes. The BSW and BSSW modes enable high sensitivity and size-selective sensing of both large surface-bound molecules and small molecules that infiltrate the pores. The BSW mode demonstrated a 6-fold improvement in detecting large molecules when compared to BSSW and WG modes. The novel BSSW mode demonstrated ~33% enhancement in small molecule sensitivity when compared to a WG mode, owing to the improved field overlap and full use of the porous matrix in both core and evanescent field regions. The BSSW can be further optimized for size selectivity and sensitivity. This work establishes a new platform for rapid, high sensitivity, label-free, and size-selective sensing at the nanoscale. The potential to further optimize the refractive index gradient or multilayer design could further improve the sensitivity or size selectivity presented here. The pore sizes of the layers responsible for supporting the BSSW mode may

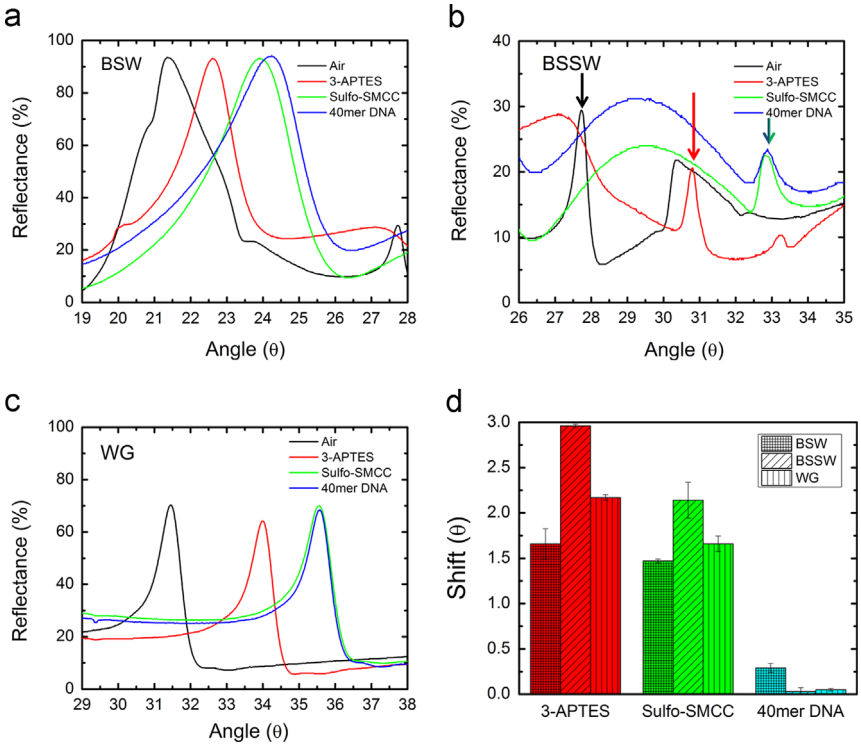

Fig. 6. Angle-resolved reflectance spectra after small and large molecule attachment in PSi (a) BSW, (b) BSSW, and (c) WG structures. The arrows shown in (b) highlight the BSSW mode. (d) Comparison of the BSW, BSSW, and WG detection sensitivity to different molecules, normalized by the initial resonance angle as described in Section 2.

also be tuned to enable size selectivity at specific depths of interest within the structure or to demonstrate infiltration uniformity of a target molecule in the porous membrane in a microfluidics based approach.

Acknowledgments

This work was supported in part by the Army Research Office (W911NF-09-1-0101), National Science Foundation (ECCS-0746296), and the Vanderbilt Institute of Nanoscale Science and Engineering (NSF ARI-R2 DMR-0963361). The authors thank Marco Liscidini and John Sipe for useful discussions. J.D.R. acknowledges support from an NSF Graduate Research Fellowship.

References

Adhikari, B., Majumdar, S., 2004. Polymers in sensor applications. Prog. Polym. Sci. 29 (7), 699–766.

Chan, S., Fauchet, P.M., Li, Y., Rothberg, L.J., Miller, B.L., 2000. Porous silicon microcavities for biosensing applications. Phys. Stat. Sol. (a) 182, 541–546.

Clare, B.H., Abbott, N.L., 2005. Orientations of nematic liquid crystals on surfaces presenting controlled densities of peptides: amplification of protein-peptide binding events. Langmuir 21 (14), 6451–6461.

Dancil, K.-P.S., Greiner, D.P., Sailor, M.J., 1999. A porous silicon optical biosensor: detection of reversible binding of IgG to a protein A-modified surface. J. Am. Chem. Soc. 121 (34), 7925–7930.

Descrovi, E., Sfez, T., Quaglio, M., Brunazzo, D., Dominici, L., Michelotti, F., Herzig, H. P., Martin, O.J.F., Giorgis, F., 2010. Guided Bloch surface waves on ultrathin polymeric ridges. Nano Lett. 10 (6), 2087–2091.

Feng, J., Zhao, W., Su, B., Wu, J., 2011. A Label-free optical sensor based on nanoporous gold arrays for the detection of oligodeoxynucleotides. Biosens. Bioelectron. 30, 21–27.

Guillermain, E., Lysenko, V., Orobtchouk, R., Benyattou, T., Roux, S., Pillonnet, A., Perriat, P., 2007. Bragg surface wave device based on porous silicon and its application for sensing. Appl. Phys. Lett. 90, 241116, http://dx.doi.org/10.1063/1.2747671.

Homola, J., Vaisocherova, H., Dostalek, J., Piliarik, M., 2005. Multi-analyte surface plasmon resonace biosensing. Methods 37, 26–36.

Jamois, C., Li, C., Orobtchouk, R., Benyattou, T., 2010. Slow Bloch surface wave devices on porous silicon for sensing applications. Photonics Nanostr.– Fundam. Appl. 8 (2), 72–77.

Jane, A., Dronov, R., Hodges, A., Voelcker, N.H., 2009. Porous silicon biosensors on the advance. Trends Biotechn. 27 (4), 230–239.

Jiao, Y., Weiss, S.M., 2010b. Design parameters and sensitivity analysis of polymer-cladded porous silicon waveguides for small molecule detection. Biosens. Bioelectron. 25, 1535–1538.

Jones, T.P., Porter, M.D., 1988. Optical pH sensor based on the chemical modification of a porous polymer film. Anal. Chem. 60, 404–406.

Kang, C., Weiss, S.M., Vlasov, Y.A., Assefa, S., 2012. Optimized light-matter interaction and defect hole placement in photonic crystal cavity sensors. Opt. Exp. 37, 2850–2852.

Khardani, M., Bouaicha, M., Bessais, B., 2007. Bruggeman effective medium approach for modelling optical properties of porous silicon: comparison with experiment. Phys. Stat. Sol. (c) 4 (6), 1986–1990.

Konopsky, V.N., Alieva, E.V., 2007. Photonic crystal surface waves for optical biosensors. Anal. Chem. 79, 4729–4735.

Lalanne, P., Mias, S., Hugonin, J.P., 2004. Two physical mechanisms for boosting the quality factor to cavity volume ratio of photonic crystal microcavities. Opt. Exp. 12 (3), 458–467.

Lawrie, J.L., Jiao, Y., Weiss, S.M., 2010. Size-dependent infiltration and optical detection of nucleic acids in nanoscale pores. IEEE Trans. Nanotechnol. 9 (5), 596–602.

Li, S., Hu, D., Huang, J., Cai, L., 2012. Optical sensing nanostructures for porous silicon rugate filters. Nanoscale Res. Lett. 7 (79), 1–8.

Liscidini, M., Galli, M., Patrini, M., Loo, R.W., Goh, M.C., Ricciardi, C., Giorgis, F., Sipe, J.E., 2009. Demonstration of diffraction enhancement via Bloch surface waves in a-SiN:H multilayers. Appl. Phys. Lett. 94 (4), 043117, http://dx.doi.org/10.1063/1.3076101.

Liscidini, M., Sipe, J.E., 2009. Analysis of Bloch-surface-wave assisted diffraction-based biosensors. J. Opt. Soc. Am. B 26, 279–289.

Maxwell, D.J., Taylor, J.R., Nie, S., 2002. Self-assembled nanoparticle probes for recognition and detection of biomolecules. J. Am. Chem. Soc. 124 (32), 9606–9612.

Michelotti, F., Sciacca, B., Dominici, L., Quaglio, M., Descrovi, E., Giorgis, F., Geobaldo, F., 2010. Fast optical vapour sensing by Bloch surface waves on porous silicon membranes. Phys. Chem. Chem. Phys. 12 (2), 502–506.

Moharam, M.G., Grann, E.B., Pommet, D.A., Gaylord, T.K., 1995. Formulation for stable and efficient implementation of the rigorous coupled-wave analysis of binary gratings. J. Opt. Soc. Am. A 12 (5), 1068–1076.

Ouyang, H., Striemer, C.C., Fauchet, P.M., 2006. Quantitative analysis of the sensitivity of porous silicon optical biosensors. Appl. Phys. Lett. 88 (16), 163108, http://dx.doi.org/10.1063/1.2196069.

Pacholski, C., Sartor, M., Sailor, M.J., Cunin, F., Miskelly, G.M., 2005. Biosensing using porous silicon double-layer interferometers: reflective interferometric fourier transform spectroscopy. J. Am. Chem. Soc. 127 (33), 11636–11645.

Paeder, V., Musi, V., Hvozdara, L., Herminjard, S., Herzig, H.P., 2011. Detection of protein aggregation with a bloch surface wave based sensor. Sens. Actuators B 157, 260–264.

Pirotta, S., Xu, X.G., Delfan, A., Mysore, S., Maiti, S., Dacarro, G., Patrini, M., Galli, M., Guizzetti, G., Bajoni, D., Sipe, J.E., Walker, G.C., Liscidini, M., 2013. Surface-enhanced Raman scattering in purely dielectric structures via Bloch surface waves. J. Phys. Chem. C 117, 6821–6825.

Qiao, H., Guan, B., Gooding, J.J., Reece, P.J., 2010. Protease detection using a porous silicon based Bloch surface wave optical biosensor. Opt. Exp. 18 (14), 15174–15182.

Rong, G., Najmaie, A., Sipe, J.E., Weiss, S.M., 2008. Nanoscale porous silicon waveguide for label-free DNA sensing. Biosens. Bioelectron. 23, 1572–1576.

Ryckman, J.D., Liscidini, M., Sipe, J.E., Weiss, S.M., 2010. Porous silicon structures for low-cost diffraction-based biosensing. Appl. Phys. Lett. 96, 171103, http://dx.doi.org/10.1063/1.3421545.

Sinibaldi, A., Danz, N., Descrovi, E., Munzert, P., Schulz, U., Sonntag, F., Dominici, L., Michelotti, F., 2012. Direct comparison of the performance of bloch surface wave and surface plasmon polariton sensors. Sens. Actuators B Chem. 174, 292–298.

Snow, P.A., Squire, E.K., Russel, P.S.J., Canham, L.T., 1999. Vapor sensing using the optical properties of porous silicon Bragg mirrors. J. Appl. Phys. 86, 1781, http://dx.doi.org/10.1063/1.370968.

Toma, K., Descrovi, E., Toma, M., Ballarini, M., Mandracci, P., Giorgis, F., Mateescu, A., Jonas, U., Knoll, W., Dostalek, J., 2013. Bloch surface wave-enhanced fluorescence biosensor. Biosens. Bioelectron. 43, 108–114.

Wei, X., Kang, C., Liscidini, M., Rong, G., Retterer, S.T., Patrini, M., Sipe, J.E., Weiss, S. M., 2008. Grating couplers on porous silicon planar waveguides for sensing applications. J. Appl. Phys. 104, 123113–123117.

Wei, X., Mares, J.W., Gao, Y., Li, D., Weiss, S.M., 2012. Biomolecule kinetics measurements in flow cell integrated porous silicon waveguides. Biomed. Opt. Exp. 3 (9), 1993–2003.

Wei, X., Weiss, S.M., 2011. Guided mode biosensor based on grating coupled porous silicon waveguide. Opt. Exp. 19 (12), 11330–11339.

Zhu, M., Lerum, M.Z., Chen, W., 2012. How to prepare reproducible, homogeneous, and hydrolytically stable aminosilane-derived layers on silica. Langmuir 28 (1), 416–423.